Geometric stochastic resonance in a double cavity

Pulak K. Ghosh,[1] Russell Glavey,[2] Fabio Marchesoni,[3, 1] Sergey E. Savel'ev,[2, 1] and Franco Nori[1, 4]

[1]*Advanced Science Institute, RIKEN, Wako-shi, Saitama, 351-0198, Japan*
[2]*Department of Physics, Loughborough University, Loughborough LE11 3TU, United Kingdom*
[3]*Dipartimento di Fisica, Università di Camerino, I-62032 Camerino, Italy*
[4]*Department of Physics, University of Michigan, Ann Arbor, MI 48109-1040, USA*
(Dated: March 6, 2013)

Geometric stochastic resonance of particles diffusing across a porous membrane subject to oscillating forces is characterized as a synchronization process. Noninteracting particle currents through a symmetric membrane pore are driven either perpendicular or parallel to the membrane, whereas harmonic-mixing spectral current components are generated by the combined action of perpendicular and parallel drives. In view of potential applications to the transport of colloids and biological molecules through narrow pores, we also consider the role of particle repulsion as a controlling factor.

I. INTRODUCTION

Historically, research on Stochastic Resonance (SR) [1] focused mostly on systems with purely energetic potentials, either continuous or discrete. However, as pointed out in Ref. [2], in soft condensed matter and in a variety of biological systems [3, 4], particles are often confined to constrained geometries, such as interstices, pores, or channels, whose size and shape can affect the SR mechanism [5]. Indeed, smooth confining geometries can be modeled as entropic (i.e., noise or temperature dependent) potentials [6], capable of influencing the response of the system to an external driving force (see, for a review, Ref. [7]).

A more interesting scenario emerges in the case of sharp confining geometries. In a recent paper [8] we showed that a Brownian particle confined to two distinct cavities divided by a porous medium, say a membrane, undergos SR when driven by an ac force perpendicular to the membrane. This means that, at variance with ordinary SR [1], optimal synchronization between drive and particle oscillations for an appropriate noise level, occurs even in the *absence* of a bistable effective potential, of either energetic or entropic nature [5]. However, such a manifestation of SR in higher dimensions requires adopting extremely sharp geometrical constrictions to separate the two cavities. The magnitude and conditions of such a *geometric* SR effect are sensitive to the geometry of the cavities and the structure of the pores.

This instance geometric SR should not be mistaken for the socalled *entropic* SR introduced in Ref. [5], where the Brownian particle can switch cavity only by overcoming the entropic barrier determined by the geometric constriction associated with a smooth pore. In the absence of an energetic barrier, the entropic barrier alone determines the magnitude of the SR effect that occurs when a periodic force drives the particle across the pore, although the evidence reported by Burada *et al.* [5] hints at an interplay of entropic and energetic barriers, rather than to a mere entropic effect.

Geometric SR is a peculiar manifestation of driven Brownian motion in septate channels [9–13]. In these channels compartments are separated by zero-thickness partition walls and the pores are modeled by structureless holes pierced at the center of the partition walls. A septate channel cannot be analyzed in terms of the reductionist approach of Ref. [6], i.e., as entropic channels [2, 7], because the geometry of its pores turns out to be too sharp for a one dimensional (1D) kinetic equation approximation to hold [14]. However, sharp pore geometries are known to enhance most of the noise controlled transport mechanisms proposed in recent years [4], thus making this class of channels particularly suitable for experimental demonstrations.

In this paper we restrict our analysis to two dimensional (2D) geometries. Our choice is partly motivated by the growing interest in vortex superconducting devices, a class of artificial devices with numerous technological applications, including flux qubits, SQUIDs and superconducting rf filters [15, 16]. Superconducting samples with two vortex boxes connected by a thin pore of almost any geometry can be easily fabricated. Vortices are trapped inside the boxes with binding energy of the order of $\Phi_0^2 L_t / \lambda^2$, where Φ_0 is the magnetic flux quantum, λ is the London penetration depth, and L_t is the depth of the two vortex traps. Magnetic vortices repel one another through a logarithmic pair potential, while their density, $n = H/\Phi_0$, is controlled by the intensity H of the applied magnetic field. In the dilute limit, $H \lesssim \Phi_0/\lambda^2$, the vortex-vortex interactions become negligible, so that the transport properties of a single trapped vortex are not overshadowed by many-body effects. ac drives and noise sources can be easily implemented as Lorentz forces generated by independent electric currents injected into the sample parallel and perpendicular to the pore axis. Detection of SR under such experimental conditions is thus regulated by the applied current sources only; in particular, the noise parameter can be varied independently of the constant operating sample temperature.

This paper is organized as follows. In Sec. II we summarize the spectral properties of geometric SR, as first reported in Ref. [8]. In Sec. III we analyze geomet-
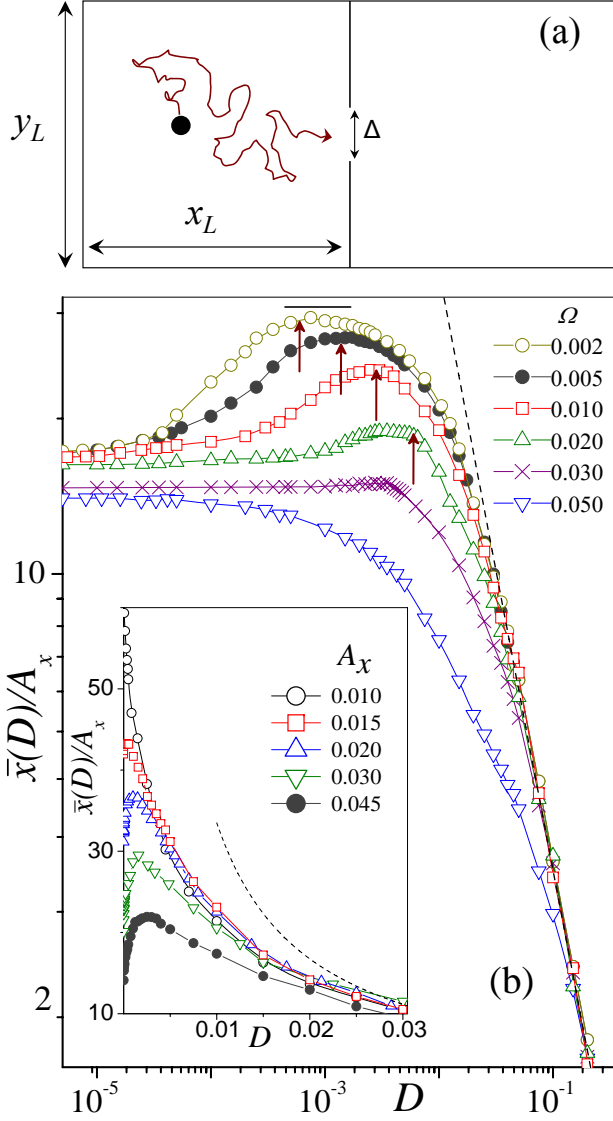
FIG. 1: (Color online) (a) Brownian particle confined to a 2D box divided in two compartments by a partition with an opening of width Δ at the center. (b) Geometric stochastic resonance. $\overline{x}(D)$ versus D for different values of Ω at $A_0 = 0.045$ (main panel) and A_x at $\Omega = 0.01$ (inset). Other parameters are: $x_L = y_L = 1$ and $\Delta = 0.1$. In the inset we also report our predictions for the SR peak position $D_{\max}$ (vertical arrows) and height $\overline{x}(D_{\max})$ (top line). In both plots the dashed line represents the decay law $\overline{x}(D \to \infty)$ (see Sec. II).

ric SR as a noise controlled synchronization mechanism. The distribution of the crossing times of a single particle through a pore is investigated in the case of both longitudinal and transverse ac drives. In Sec. IV we study the particle current through a pore under the combined action of longitudinal and transverse drives with incommensurate frequencies. Harmonic mixing is detected as a consequence of confinement, even in the absence of nonlinear particle interactions. In Sec. V we explore the role of particle repulsion in controlling geometric SR, by varying the particle density and the pair interaction intensity. Finally, in Sec. VI we add some concluding remarks.

II. GEOMETRIC STOCHASTIC RESONANCE

Let us consider an overdamoed Brownian particle freely diffusing in a 2D suspension fluid contained in two symmetric $x_L \times y_L$ compartments, with reflecting walls [17], connected by a narrow pore of width Δ, as illustrated in Fig. 1(a). The overdamped dynamics of the particle is modeled by the Langevin equation,

$$\frac{d\vec{r}}{dt} = -\vec{A}(t) + \sqrt{D}\ \vec{\xi}(t), \qquad (1)$$

where $\vec{A} = (A_x, A_y)$ are the x, y components of the driving force and $\vec{\xi}(t) = (\xi_x(t), \xi_y(t))$ are zero-mean, white Gaussian noises with autocorrelation functions $\langle \xi_i(t)\xi_j(t') \rangle = 2\delta_{ij}\delta(t - t')$, with $i, j = x, y$. Equation (1) has been numerically integrated by a Milstein algorithm [18]. Stochastic averages were obtained as ensemble averages over 10^6 trajectories with random initial conditions; transient effects were estimated and subtracted.

In the presence of a longitudinal ac drive oriented along the x axis, $A_x(t) = A_x \cos(\Omega t)$, the Brownian trajectories embed a persistent harmonic component, $\overline{x}(D) \cos[\Omega t - \phi(D)]$, whose amplitude, $\overline{x}$ is plotted versus D in Fig. 1(b). For details about the curves $\phi(D)$, not relevant to the discussion below, the reader is referred to the original paper [8].

The occurrence of geometric SR is clearly documented in Ref. [8]. Its main distinctive properties that can be summarized as follows:

(i) $\overline{x}(D)$ peaks for an appropriate noise intensity, $D_{\max}$, with upper bound,

$$\overline{x}(D_{\max}) \leq \frac{4}{\pi}\ x_L. \qquad (2)$$

A satisfactory estimate of $D_{\max}$ was obtained by matching the half-drive period with mean first-exit time from one compartment at $A_x = 0$, $\tau_\Delta(D)$, that is,

$$\tau_\Delta(D_{\max}) = \frac{T_\Omega}{2} \equiv \frac{\pi}{\Omega}. \qquad (3)$$

Note that $\tau_\Delta(D)$ is inversely proportional to D and strongly depends on the pore width, Δ, as computed in Ref. [12]. Hence, $D_{\max}$ is proportional to Ω;

(ii) SR is restricted to $A_0 > A_c$ or $\Omega < \Omega_c$, as a consequence of the geometric condition,

$$\frac{A_x}{\Omega} \geq \frac{4}{\pi}\ x_L. \qquad (4)$$

This is an important difference with respect to ordinary SR [1], where there exist no such onset thresholds in the drive parameters space;

(iii) $\bar{x}(D)$ obeys the approximate SR curve,

$$\bar{x}(D) = \frac{\bar{x}_0(D)}{\sqrt{1 + [\Omega \tau_\Delta(D)]^2}}, \qquad (5)$$

where,

$$\bar{x}_0(D) = \frac{A_x x_L/D}{\tanh(A_x x_L/D)} - 1, \qquad (6)$$

is the amplitude of the $\langle x(t) \rangle$ oscillations in the adiabatic limit $\Omega \to 0$. As a consequence, for large noise, $\bar{x}(D) \propto 1/D$.
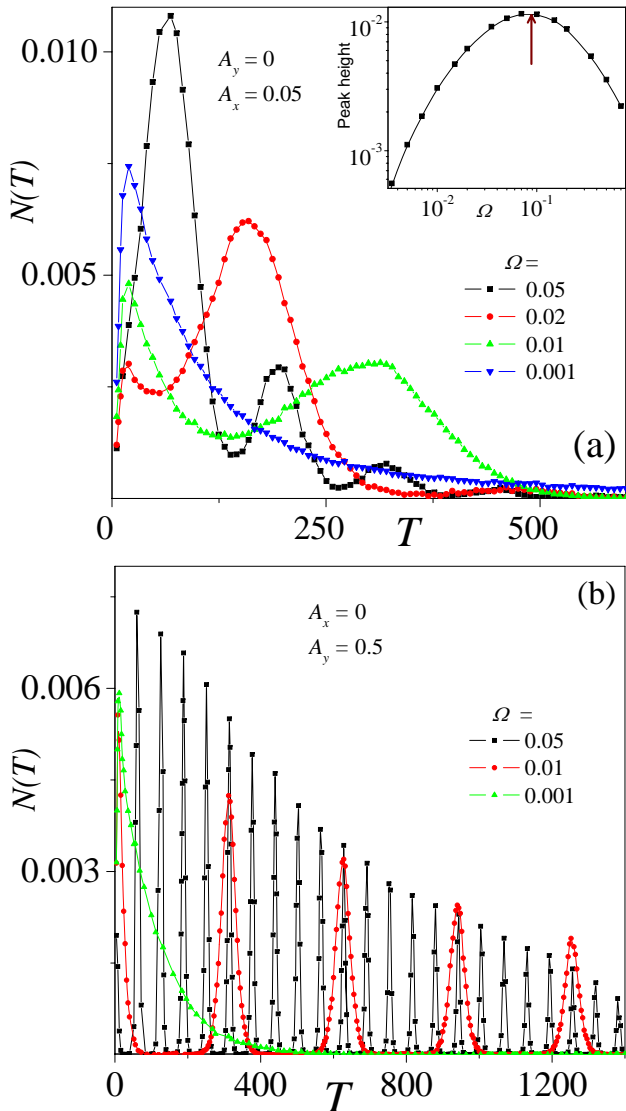

(a)

(b)

FIG. 2: (Color online) Synchronization mechanism. Distribution density of the residence times for different periods $T_\Omega = 2\pi/\Omega$ (in the legends) of the (a) longitudinal drive with $A_x = 0.05$ and (b) transverse drive with $A_y = 0.5$. The cavity dimensions are as in Fig. 1 and $D = 0.015$. Inset in (a): height of the first peak, $n = 1$, versus Ω. Vertical arrow denotes the resonant Ω value predicted in Eq. (8) with τ_Δ given in [12].

The properties listed above follow from simple geometrical considerations. Equation (3) is the *geometric counterpart of the standard SR condition* [1], where, in the absence of an energetic barrier, the Arrhenius time is replaced by an appropriate diffusion time across the pore. As is apparent in Eq. (6), for weak noise and low drive frequencies, $A_x(t)$ presses the particle against the walls of the container opposite to the dividing wall and, as a result, the average particle displacement, $\langle x(t) \rangle$, approaches a square waveform with amplitude x_L. The amplitude of the Fourier component of $\langle x(t) \rangle$ with angular frequency Ω is then, $4x_L/\pi$. From this remark it immediately follow the inequalities in Eqs. (2) and (4), A_x/Ω being the driven oscillation amplitude of an unconstrained Brownian particle. The upper bound of Eq. (2) hold for vanishingly low Ω, see Fig. 1(b). For stronger noise but still low drive frequencies, $\bar{x}_0(D)$ tends to $A_x \tau_x$, where $\tau_x = x_L^2/3D$ is the longitudinal diffusion time across a cavity compartment. The pore effectively suppresses the particle oscillations, with damping constant $\tau_\Delta(D)^{-1}$, only at relatively high drive frequencies, as apparent from Eq. (5). The consistency of these analytical results with the simulations is quite satisfactory, as shown in [8].

III. SYNCHRONIZATION MECHANISMS

As summarized in Sec. II, the evidence for geometric SR reported in Ref. [8] focuses on the D dependence of the harmonic component of $\langle x(t) \rangle$ with driving frequency Ω. This spectral characterization of geometric SR will be further discussed in the following section.

An alternative and perhaps deeper insight into the underlying resonance mechanism can be gained by considering the so-called synchronization characterization of SR [19]. In this approach one looks at the residence times, T, of the Brownian particle in either cavity – which one is irrelevant, due to the mirror symmetry of the process with respect to the cavity divide. Their distribution densities, $N(T)$, exhibit a prominent peak structure and, more remarkably, a resonating D and T dependence.

A. Longitudinal drive

Let us consider first the case of longitudinal drives, $A_y = 0$. In Fig. 2(a) we plotted $N(T)$ for different values of Ω at constant D. It is immediately apparent that the $N(T)$ peaks are centered around

$$T_n = \left(n - \frac{1}{2}\right) T_\Omega, \quad n = 1, 2, 3, \ldots, \qquad (7)$$

due to the fact that the left-to-right pore crossings are most likely to occur when the longitudinal ac force $A_x(t)$ points to the right and vice versa. Such a synchronization mechanism has been discussed at length in the SR

literature [1]. A detailed numerical analysis (shown in Fig. 2(a) for $n = 1$) proves that the height of (or, more precisely, the area enclosed under) the n-th distribution peak increases with Ω up to an optimal value $\Omega = \Omega_n$, and then decreases for higher Ω. Note that Ω_n is determined by the optimal synchronization condition [19]

$$\left(n - \frac{1}{2}\right) T_\Omega = \tau_\Delta(D), \quad n = 1, 2, 3, \ldots. \quad (8)$$

Note that for $n = 1$ this equality coincides with the spectral SR condition in Eq. (3). This proves that the first peak (but this conclusion actually applies to all them!) can be enhanced to a maximum by acting either upon T_Ω or τ_Δ. Hence, geometric SR is also a *bona-fide* resonance [19].

B. Transverse drive

We now consider the case of transverse drives, $A_x = 0$. Clearly, a drive parallel to the compartment wall of the cavity in Fig. 1(a) cannot break the mirror symmetry of the system in the x direction. However, it impacts the diffusion process through the pore, in that it presses the Brownian particle periodically against the horizontal walls, twice a period. Pressed against the top and the bottom walls of the cavity, symmetrically placed with respect to the pore, the particle is less likely to escape the side of the cavity it is trapped in; it is more likely to do so as $A_y(t)$ reverses sign, twice a period. Therefore, one expects $N(T)$ to develop a denser peak structure with

$$T_n = \frac{n}{2} T_\Omega, \quad n = 1, 2, 3, \ldots, \quad (9)$$

as shown in Fig. 2(b). Analogously to the situation of Fig. 2(a), the distribution peaks become sharpest for an optimal value of Ω. An explicit numerical analysis (not shown) confirms that such an optimal synchronization occurs also under the resonance condition of Eq. (8), but with the difference that now $\tau_\Delta(D)$ stays for the transverse diffusion time $\tau_y = y_L^2/3D$. Although the right and left flows through the pore are modulated in time, we stress that in the presence of a transverse drive $A_y(t)$, no geometric SR can occur because of the persistent mirror symmetry of the longitudinal motion.
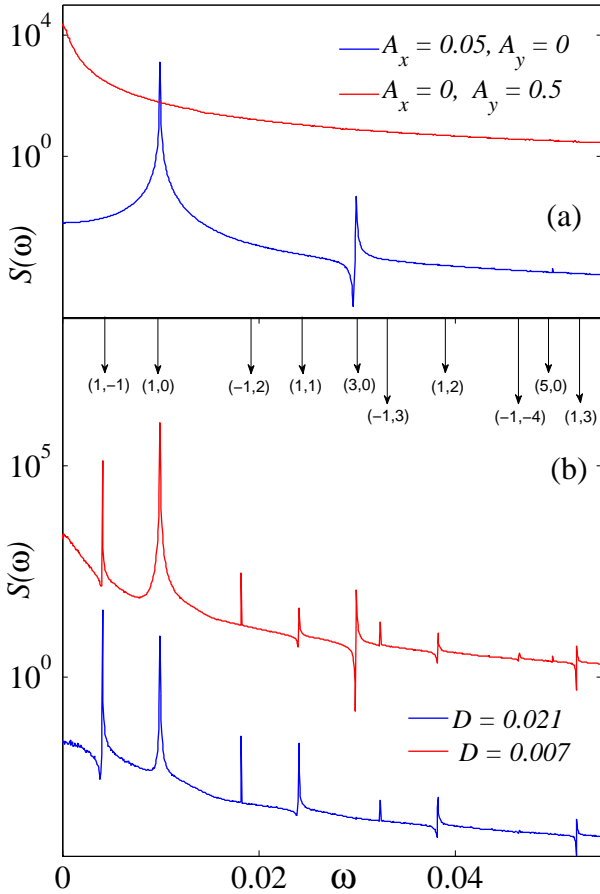

FIG. 3: (Color online) Harmonic mixing in a cavity. Spectral density of the coordinate $x(t)$ for two different noise intensities, D, and (a) either a longitudinal or a transverse drive (see legend); (b) a combination of longitudinal and transverse drives. The drive parameters are $A_x = 0.05$, $A_y = 0.5$, $\Omega_x = 0.01$, and $\Omega_y = \Omega_x/\sqrt{2}$. The harmonic mixing resonances are indicated by down-pointing vertical arrows with relevant indices (m, n).
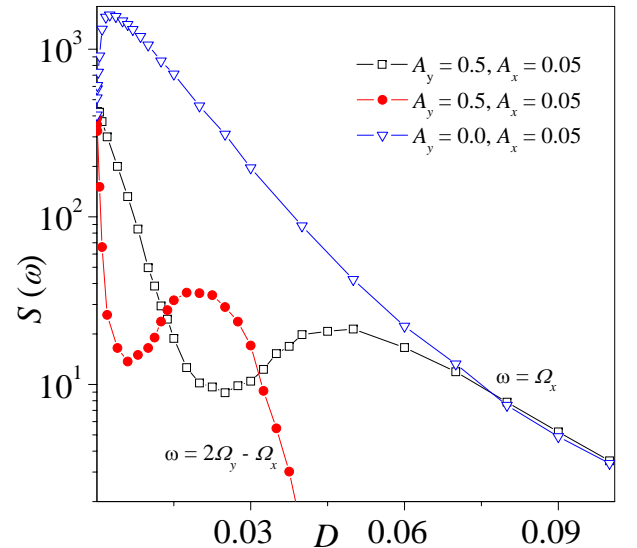

FIG. 4: (Color online) Resonant behavior of the two lowest order harmonic mixing components $(1,0)$, $(-1,1)$. For the sake of comparison $S(\omega_{1,0})$, is shown also for $(A_x, A_y) = (0.005, 0)$, geometric SR. All simulation parameters here are as in Fig. 3(b).

IV. HARMONIC MIXING

The spectral characterization of geometric SR, as outlined in Sec. II, can provide us with more insight into the resonant transport mechanisms at work in a partitioned cavity. The analysis of Ref. [8] is equivalent to taking the power spectral density (PSD) of $x(t)$, $S(\omega)$, and evaluating the δ-like spike, $(\pi/2)\bar{x}^2(D)\delta(\omega - \Omega)$, corresponding to the harmonic component of $\langle x(t) \rangle$ with frequency Ω. As clearly shown in Fig. 3(a), $S(\omega)$ develops a series of spectral spikes at

$$\omega_n = (2n - 1)\,\Omega, \quad n = 1, 2, 3, \ldots. \quad (10)$$

As well known from the SR literature [1], the even harmonics of the driving frequency are absent as a consequence of the $x \to -x$ symmetry of the 2D Langevin equation (1). On the other hand, as anticipated in the final paragraph of Sec. III, SR cannot be induced by transverse drives. As expected, the PSD for $A_x = 0$ and $A_y \neq 0$ displayed in Fig. 3(a) exhibits no resonance spike.

More interesting is the situation of Fig. 3(b), where the Brownian particle is subjected to drives in both directions. The intrinsic nonlinearity of the longitudinal and transverse flows discussed in Sec. IIIA and B makes a mixing between them possible, a phenomenon called harmonic mixing (HM).

As discussed in Ref. [20], key ingredients for HM in a 1D nonlinear system are: (i) nonlinearity of the driven process; (ii) combination of at least two harmonic drives with angular frequencies Ω_1 and Ω_2; (iii) commensuration of the driving frequencies, that is, $\Omega_1/\Omega_2 = p/q$, with p ad q relative prime numbers. Under such conditions, the system response to the external drives develops a hierarchy of harmonics at

$$\omega_{m,n} = m\Omega_1 + n\Omega_2 \quad m, n = 0, \pm 1, \pm 2, \ldots. \quad (11)$$

Dynamical symmetries peculiar to the system can lead to the suppressions of subsets of the harmonics $\omega_{m,n}$.

The system investigated in this section, however, is two dimensional, which means that HM can occur for any ratio of the driving frequencies. In our simulations we employed orthogonal harmonic drives, $A_x(t)$ and $A_y(t)$, with incommensurate frequencies, Ω_x and Ω_y. We know from Sec. III that the longitudinal flows driven by the transverse force alone can only resonate at the *even* harmonics of Ω_y, namely for $\omega = 2n\Omega_y$, $n = 1, 2, 3, \ldots$. This is an effect of the mirror symmetry of the cavity with respect to the horizontal axis passing through the center of the pore. Moreover, as mentioned above, the mirror symmetry of the cavity with respect to its compartment wall restricts the periodic components of $\langle x(t) \rangle$ to the *odd* harmonics of $A_x(t)$, i.e., $\omega = (2n - 1)\Omega_x$, $n = 1, 2, 3 \ldots$.

In conclusion, the HM spectrum of the longitudinal flow through the cavity pore is expected to be

$$\omega_{m,n} = m\Omega_x + 2n\Omega_y \quad (12)$$

with $m = \pm 1, \pm 3, \pm 5, \ldots$ (odd) and $n = 0, \pm 1, \pm 2, \ldots$, with no commensuration condition on the ratio Ω_x/Ω_y. Our prediction is corroborated by the PSD. curves plotted in Fig. 3(b): Ω_x/Ω_y is an irrational number and, still, all detectable spectral peaks could be identified by a pair of indices (m, n) according to Eq. (12).

The practical implications of the HM of longitudinal and transverse drives is that, while the time modulation introduced by the harmonic signal $A_y(t)$, alone, cannot be picked up by the longitudinal current across a pore, adding a small longitudinal signal makes $A_y(t)$ detectable through the very same observable. We also stress that mixing spikes with $n, m \neq 0$ are not necessarily small
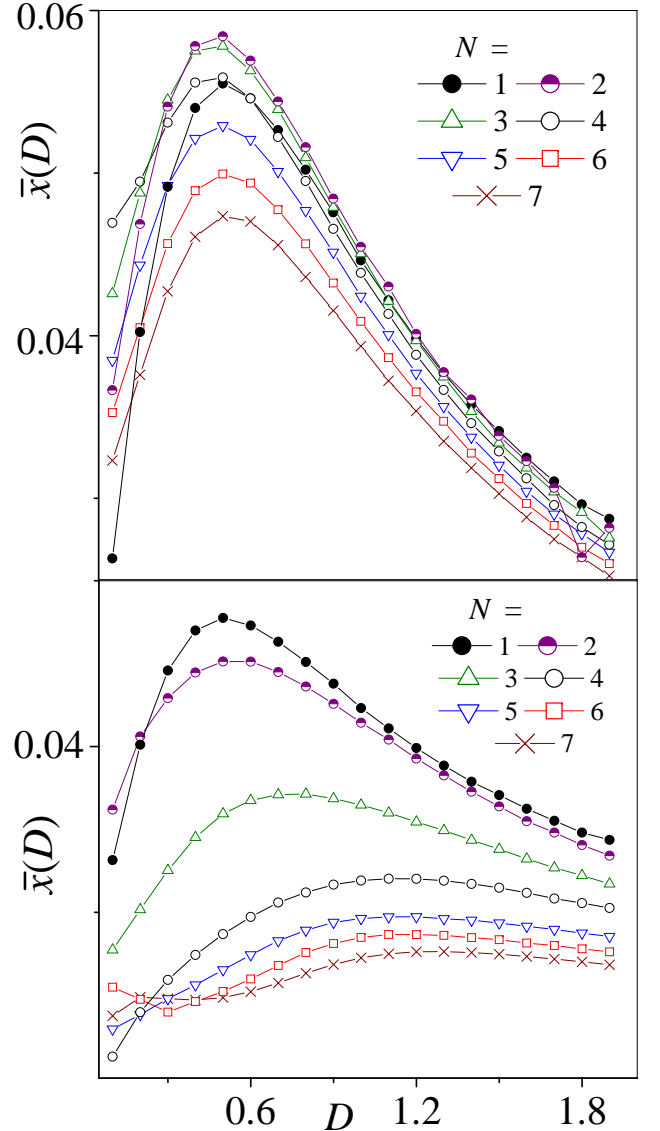

FIG. 5: (Color online) Geometric SR for interacting particles. $\bar{x}(D)$ versus D for the double cavity shown in Fig. 1 for N identical particles repelling via the pair force of Eq. (13) with $\alpha = 1$ (a) and 6 (b). The drive parameters are $A_x = 0.05$, $A_y = 0$, and $\Omega_x = 0.01$.

with respect to the harmonics of the longitudinal signal, $n = 0$. In fact, all PSD spikes, $S(\omega_{m,n})$ manifest a SR dependence of their own on the noise intensity. For instance, in Fig. 4, for an appropriate D range, the HM harmonics $(-1, 1)$ overshoots the fundamental component $(1, 0)$.

V. PARTICLE INTERACTION

To further explore the effects of the confining geometry on the pore crossing mechanism, we consider now the role of particle interaction. We assume that N Brownian particles are randomly distributed between the two cavities of the system and repel one another through the standard vortex-vortex potential [16],

$$f_{i,j} = \frac{\alpha}{|\vec{r_i} - \vec{r_j}|}, \qquad (13)$$

where $i, j = 1, 2, \ldots, N$ and $i \neq j$. The situation modeled here is recurrent in biological physics [3, 6–10], where constrained geometries often accommodate controllable concentrations of suspended particles. The exact form of $f_{i,j}$ is not relevant to the present discussion [21]. Here we address the dependence of the geometric SR on the parameters N (concentration) and α (coupling) of a system of interacting particles.

Let us consider the geometry SR setup of Sec. II with a longitudinal harmonic drive, $A_x(t)$, of fixed angular frequency Ω_x. In Fig. 5 we plot the curves $\bar{x}(D)$ for low
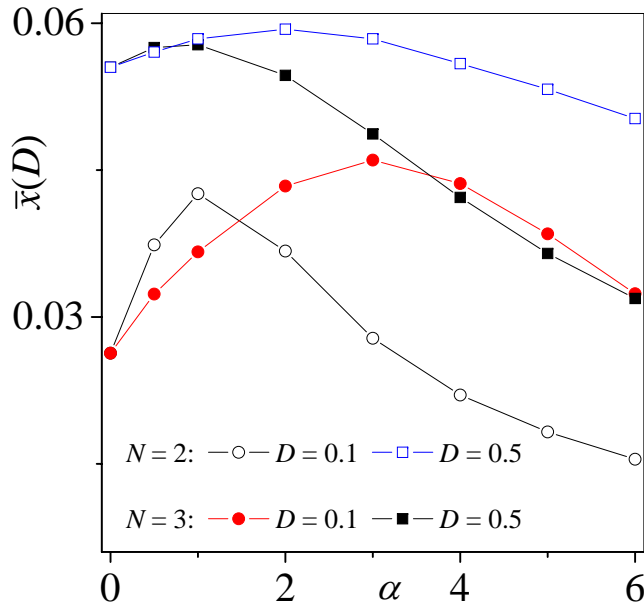

FIG. 6: (Color online) $\bar{x}(D)$ versus α for the same setup as in Fig. 5 with N and D fixed (see legend). The parameter α is the strength of the particle-particle interaction. $\bar{x}(D)$ shows a peak for relatively small values of α, and slowly decreases for laser values of α.

α, in panel (a), and large α, in panel (b), and increasing particle concentrations. For low α, increasing N amounts to reducing the effective cavity volume accessible to the Brownian particles. Moreover, when the particle coupling is relatively weak, their interactions only exert a mean field effect on the pore crossing process. As a consequence, one expects that, in the regime of low couplings, the SR noise intensity, $D_{\max}$ in Eq. (3), weakly depends on N, whereas the height of the SR peak, Eq. (2), diminishes with raising N. This description interprets qualitatively well the results of Fig. 5(a). An exception is represented by the curve with $N = 1$, which lies under the curve with $N = 2$ and peaks at higher D. All the remaining curves are centered around the same $D_{\max}$, their maxima slowly decreasing for increasing N, with $N > 2$. As a matter of fact, when passing from $N = 1$ to $N = 2$, pair repulsion clearly makes pore crossing more effective than for a single particle. However, as argued above, this effect becomes negligible when adding one particle at larger N.

For large α, as shown in Fig. 5(b), the pair repulsion can grow so strong that pair crossings become unlikely. Cavity switching can only be achieved by pumping more noise into the system, which means that the SR peaks must shift to higher $D_{\max}$ for larger concentrations. Of course, for very large N, the harmonic component of $\langle x(t) \rangle$ is suppressed independent of the value of α.

The α dependence of the driven flow across the pore is further illustrated in Fig. 6 for $N = 2$ and $N = 3$. The curves for low noise, say, $D < D_{\max}$ for $\alpha = 0$, are particularly suggestive. The noise is so small that in the absence of interactions pore crossing happens with a time constant substantially larger than a half-drive period, see Eq. (3). When switching on the interaction, the accessible free volume per particle shrinks, which facilitates the escape of single particles through the pore. This explains the raising branch of the curves $\bar{x}$ versus α. As the coupling α grows stronger, particle repulsion gets global, with the consequence that particles tend to move in deformable clusters (plastic flow [22]); at exceedingly large α, cavity switching stops and $\bar{x}$ decays to zero. According with the above argument, the resonant dependence of $\bar{x}$ on α is less appreciable for higher noise levels.

VI. CONCLUSIONS

We have shown how particles suspended in a partitioned cavity can diffuse across a pore or hole in the dividing wall, subjected to the combined action of thermal fluctuations and period drives. The particle flow across the pore is time-modulated at the drives' frequencies, with amplitudes that can be optimized by controlling the temperature of the system. This is a geometric effect where the resonance condition depends on the shape of the cavity and on the interactions among the particles it contains.

The mechanism discussed in this paper clearly does

not depend on the dimensionality of the cavity (experiments, e.g., on colloidal systems, can more easily be carried out in 3D geometries), but can be affected by other competing effects: (i) Pore structure; For a finite-size particle, say, a translocating molecule, the actual crossing time varies with the wall structure inside the pore and in the vicinity of its opening [3]; (ii) Microfluidic effects: The flow of the electrolytic suspension fluid across the pore generates inhomogeneous velocity and electrical fields which act on drift and the orientation of the driven particles [7]. System-specific effects (i) and (ii) can in principle be incorporated in our model by adding appropriate potential terms to the Langevin equation (1).

Acknowledgments

[1] L. Gammaitoni, P. Hänggi, P. Jung, and F. Marchesoni, Rev. Mod. Phys. **70**, 223 (1998); for an update see L. Gammaitoni, P. Hänggi, P. Jung, and F. Marchesoni, Special issue on *Stochastic Resonance*, Eur. Phys. J. B **69**, 1 (2009) and references therein.
[2] D. Reguera, G. Schmid, P.S. Burada, J. M. Rubí, P. Reimann, and P. Hänggi, Phys. Rev. Lett. **96**, 130603 (2006).
[3] B. Hille, *Ion Channels of Excitable Membranes* (Sinauer, Sunderland, 2001); J. Kärger and D.M. Ruthven, *Diffusion in Zeolites and Other Microporous Solids* (Wiley, New York, 1992); P. Hänggi, F. Marchesoni, and F. Nori, Ann. Phys. (Leipzig) **14**, 51 (2005).
[4] P. Hänggi and F. Marchesoni, Rev. Mod. Phys. **81**, 387 (2009).
[5] P.S. Burada, G. Schmid, D. Reguera, M.H. Vainstein, J.M. Rubí, and P. Hänggi, Phys. Rev. Lett. **101**, 130602 (2008).
[6] R. Zwanzig, J. Phys. Chem. **96**, 3926 (1992); D. Reguera and J. M. Rubí, Phys. Rev. E **64**, 061106 (2001); P. Kalinay and J. K. Percus, Phys. Rev. E **74**, 041203 (2006).
[7] P.S. Burada, P. Hänggi, F. Marchesoni, G. Schmid, and P. Talkner, ChemPhysChem **10**, 45 (2009).
[8] P.K. Ghosh, F. Marchesoni, S.E. Savel'ev, and F. Nori, Phys. Rev. Lett. **104**, 020601 (2010).
[9] Yu.A. Makhnovskii, A.M. Berezhkovskii, and V.Yu. Zitserman, J. Chem. Phys. **131**, 104705 (2009).
[10] A.M. Berezhkovskii, L. Dagdug, Yu.A. Makhnovskii, and V.Yu. Zitserman, J. Chem. Phys. **132**, 221104 (2010).
[11] F. Marchesoni and S. Savel'ev, Phys. Rev. E **80**, 011120 (2009).
[12] M. Borromeo and F. Marchesoni, Chem. Phys. **375**, 536 (2010); F. Marchesoni, J. Chem. Phys. **132**, 166101 (2010).
[13] P. Hänggi, F. Marchesoni, S. Savel'ev, and G. Schmid, Phys. Rev. E **82**, 041121 (2010).
[14] M.H. Jacobs, *Diffusion Processes* (Springer, New York, 1967).
[15] B.Y Zhu, F. Marchesoni, and F. Nori, Phys. Rev. Lett. **92**, 180602 (2004).
[16] J.E. Villegas *et al.*, Science **302**, 1188 (2003); C.C. De Souza Silva *et al.*, Nature **440**, 651 (2006); S. Savel'ev, F. Nori, Nature Materials **1**, 179 (2002); Y. Togawa, *et al.*, Phys. Rev. Lett. **95**, 087002 (2005); D. Cole, *et al.*, Nature Materials **5**, 305 (2006); F. Nori, Nature Physics **2**, 227 (2006); S. Ooi *et al.*, Phys. Rev. Lett. **99**, 207003 (2007).
[17] C.W. Gardiner, *Handbook of Stochastic Methods* (Springer, Berlin, 2004).
[18] P. Kloeden and E. Platen, *Numerical Solutions of Stochastic Differential Equations* (Springer, Berlin, 1999).
[19] L. Gammaitoni, F. Marchesoni, E. Menichella-Saetta, and S. Santucci, Phys. Rev. Lett. **62**, 349 (1989); L. Gammaitoni, F. Marchesoni, and S. Santucci, Phys. Rev. Lett. **74**, 1052 (1995).
[20] F. Marchesoni, Phys. Lett. A **119**, 221 (1986); S. Savelev, F. Marchesoni, P. Hanggi, F. Nori, Europhys. Lett. **67**, 179 (2004); Phys. Rev. E **70**, 066109 (2004).
[21] S. Savel'ev, F. Marchesoni, and F. Nori, Phys. Rev. Lett. **91**, 010601 (2003); *ibid.*, **92**, 160602 (2004).
[22] C.J. Olson, C. Reichhardt, and F. Nori, Phys. Rev. Lett. **81**, 3757 (1998); F. Nori, Science **271**, 1373 (1996).